Applied Physics B (2022) 128:81
https://doi.org/10.1007/s00340-022-07806-x

Applied Physics B
Lasers and Optics

Emission spectrum characteristics of SF_6 plasma based on femtosecond laser-guided high-voltage discharge

Yungang Zhang[1] · Zheng Lu[1] · Huangtao Liu[1] · Qiang Gao[2] · Bo Li[2] · Xijun Wu[1]

Received: 26 October 2021 / Accepted: 13 March 2022 / Published online: 25 March 2022

Abstract

The detection of SF_6 decomposition products can determine the type of gas-insulated equipment failure and the degree of damage. However, the existing sampling-based detection methods cannot avoid the conversion of decomposition products, which leads to the inability to accurately establish a decomposition mechanism and diagnose insulation faults based on the decomposition products. An in situ measurement method of SF_6 decomposition products is proposed to study the decomposition characteristics of SF_6 under high-voltage discharge. First, femtosecond laser-guided high-voltage discharge is used to realize the precise control of high-voltage discharge in space and time. Space-resolved spectra generated by femtosecond laser-guided high-voltage discharge are obtained to realize the composition measurement of SF_6 decomposition products. Second, the SF_6 discharge decomposition spectra are obtained under different discharge voltages to study the effects of discharge voltages on decomposition products. Finally, the electron temperature and electron density of SF_6 plasma are studied at different voltages, the experimental results indicate that the maximum difference in excitation energy between the upper and lower energy levels of the spectral line is 1.93 eV, and the maximum electron temperature is 2519 K. Besides, the minimum electron density satisfying the LTE is $0.58 \times 10^{17}\ cm^{-3}$, and the minimum electron density obtained in the experiment is $7 \times 10^{17}\ cm^{-3}$. It is observed that the increasing discharge voltage can cause the electron density and electron temperature to increase linearly and decrease linearly, respectively, suggesting that the SF_6 plasma is in local thermal equilibrium based on the Mc Whirter criterion.

1 Introduction

SF_6 is widely used in gas-insulated switchgear (GIS) and other power equipment due to its excellent insulation and arc extinguishing properties [1–7]. However, SF_6 is prone to decomposition under discharge [3–7]. The low-fluorine sulfide generated from the decomposition will react with the micro-water, micro-oxygen and insulating materials in the equipment to form toxic and corrosive compounds such as SOF_4, SO_2F_2 and HF [3, 4], which will not only affect the normal operation of GIS equipment, but also endanger the health of on-site operators [1, 3, 4, 6]. Therefore, it is necessary to study the decomposition characteristics of SF_6, and the research results are of great significance for further research on the mechanism of SF_6 decomposition and online monitoring technology of high-voltage equipment. Previous studies have shown that the decomposition characteristics of SF_6 are closely related to the discharge energy of equipment [8, 9]. In general case, the number of SF_6 molecules is affected by high-energy electron flow and the number of SF_6 S–F bond breaks after collision is random. But in general, a higher energy electron flow will result in a higher probability of effective collision [9]. Specifically, a higher energy electron will have a higher probability of colliding with SF_6. In this case, more S–F bonds are caused to break and hence generate more low-fluorine sulfides, thereby producing more toxic and harmful substances. Therefore, the discharge energy has direct relation to the decomposition products of SF_6, which will have an adverse impact on the on-site operators and the insulation performance of the equipment. However, few studies about the influence of the discharge energy on the decomposition characteristics of SF_6 were conducted.

At present, mass spectrometry and chromatography method are used to research the decomposition

✉ Yungang Zhang
zhangyg@ysu.edu.cn

[1] College of Electrical Engineering, Yanshan University, Qinhuangdao 066004, China

[2] State Key Laboratory of Engines, Tianjin University, Tianjin 300072, China

characteristics of SF_6 by sampling and analyzing the decomposition components of SF_6 gas in GIS equipment [3–12]. However, such methods are facing challenges because some decomposition products may be transformed within a short period of time after being sampled [13], which will lead to an inaccurate and uncertain measurement [14]. Therefore, in situ measurement of SF_6 decomposition products is of great significance for studying the decomposition characteristics of SF_6 in an accurate manner. Even so, it is difficult to carry out in situ measurement of SF_6 decomposition products due to the randomness in time and space of free discharge.

In recent years, femtosecond laser-guided high-voltage discharge has attracted extensive attention [15–19], Polynkin et al. proposed the application of guiding natural lightning based on multi pulse guided discharge scheme. The results showed that the femtosecond laser-guided high-voltage discharge technology could realize the accurate control of discharge in time and space [16]. Leonov et al. studied the use of femtosecond laser pulses with low energy and high peak intensity (> 100 TW/cm^2) to guide and control sub microsecond high-voltage discharge. The magnetic field required for air and nitrogen breakdown at atmospheric pressure was measured. Direct imaging of discharge breakdown dynamics showed effective laser guidance [17]. Mé jean et al. demonstrated that the ability of ultrashort high-power laser pulses to trigger and guide high-voltage discharge could be significantly enhanced by subsequent visible nanosecond laser pulses [18]. Rodriguez et al. found that the trigger efficiency mainly depended on the spatial connection between the laser filament and the electrode and the time coincidence between the laser and the high-voltage peak. It is proved that the ionization filament generated by femtosecond terawatt laser pulse can trigger and guide high-voltage discharge. In addition, the technology has a lot of applications in various fields, such as guiding natural lightning [15], laser-triggered switching [20], and velocity measurements [21]. This technology has proven capable of controlling discharge in time and space precisely, which makes it easier to observe spatial resolved spectra. Furthermore, the characteristics of SF_6 decomposition products can be analyzed by spatial resolution spectra, and this detection method has great application prospects for studying the in situ measurement of SF_6 decomposition products. The space–time characteristics of femtosecond laser-guided high-voltage discharge have been studied in this paper, and the precise control of the discharge in time and space was realized in the first place. Then, the in situ measurement of SF_6 decomposition products was proved feasible, and the spatial resolved spectra of SF_6 decomposition products at different voltages were investigated. The electron temperature and electron density of SF_6 plasma at different voltages were studied at last.

2 Experiment

2.1 Experimental setup

The schematic of the experimental setup for femtosecond laser-guided high-voltage discharge in insulating medium SF_6 gas is shown in Fig. 1, which includes a gas jet, a femtosecond laser, a high-voltage discharge system and a detection system. The nozzle is a glass tube with a diameter of 2.5 mm, and SF_6 is controlled by S48 32/HMT thermal mass flow controller to eject from the nozzle with a flow rate of 3 m/s. The laser source is a femtosecond Ti: Sapphire laser (Spectra-Physics, Spitfire Ace) with an output wavelength of 800 nm, a pulse duration of 45 fs, a repetition frequency of 10 Hz, and a pulse energy of 7 mJ. The plasma channel (also called filament) generated by laser beam conduction through prism and focusing by lens ($f = 300$ mm) passes through SF_6 gas.

The high-voltage discharge system consists of a DC nanosecond pulsed high-voltage power supply (HVP-P20, Xi'an Smart Maple Electronic Technology Co., Ltd), an adjustable current limiting resistor (maximum value is 5 kΩ), and a pair of high-voltage electrodes. The frequency of the high-voltage power supply is 10 Hz, and both the rising and falling edges are 50 ns. The electrodes are connected to the positive and negative electrodes of the power supply, respectively, and the distance is 8 mm. The inset shows the spatial positional relationship between the nozzle, laser filament and high-voltage electrodes taken by a single-lens reflex (SLR) camera (D90, Nikon). The high-voltage electrode is close to the filament to guide the discharge, and the filament is

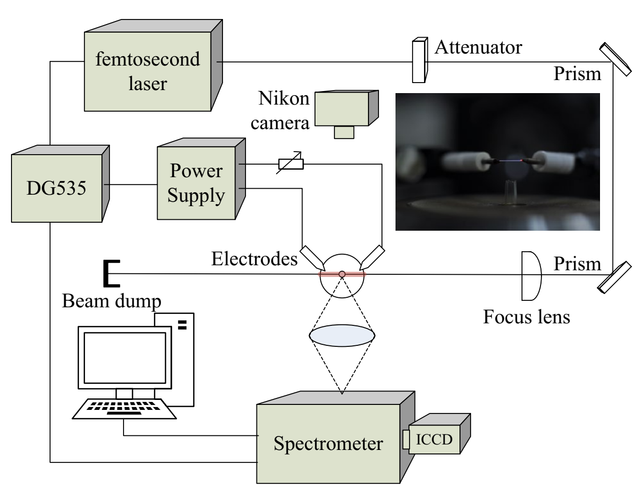

Fig. 1 Schematic diagram of experimental setup

located 2 mm directly above the nozzle. At the same time, the adjustable current limiting resistor is connected in series to control the discharge energy.

In the detection system, the scattering of the laser pulse and the emission of the discharge pulses were detected by a fast photodiode. The high-voltage probe and current probe (CT-1, Tektronix) were used to record the characteristics of the voltage and current output of the high-voltage power supply, and such data were recorded in a 600 MHz oscilloscope. A spectrometer (Acton 2300i, Princeton Instrument) equipped with a spherical lens ($f = 100$ mm) was employed to collect the plasma spectral characteristics of SF_6 decomposition products. During the measurement, the slit of the spectrometer (the slit width is 200 μm) was parallel to the plasma channel to obtain the SF_6 plasma spectrum. The signal dispersed by the grating (300 grooves/mm blazed at 300 nm) was captured at the exit port by an image-intensified charge-coupled device (ICCD, PI-MAX3: 1024i, Princeton Instruments). Before the experiment started, the wavelength of the spectrometer has been calibrated with a standard mercury lamp, and the spectral intensity has been calibrated using a standard halogen light source integrating sphere (PP-02097-000, Labsphere).

2.2 Space–time control of high-voltage discharge

Figure 2(a) shows the spatial position relationship between the electrodes and the glass nozzle, and the distance between the two electrodes is 5 mm. The arc generated high-voltage discharge without laser guidance is shown in Fig. 2(b, c), and it can be seen that a bright curve was formed between the two electrodes and the discharge path was random. Therefore, it is difficult for the discharge plasma spectrum measurement to clearly and completely image the irregular filament plasma generated by the discharge into the spectrometer, and it is also hard to synchronize the ICCD camera, which makes it extremely difficult to observe the decomposition and evolution process of SF_6.

In this experiment, the plasma channel generated by femtosecond laser self-focusing was used to realize the precise control of high-voltage discharge in space and time. The plasma channel had weak conductivity and can be used to guide discharge [15]. The plasma has a certain life, and its ability to lead discharge reduces gradually with the increase of the delay time, so it needs to have a good overlap between the life of the plasma channel and the time to reach the peak voltage across the electrodes. In this experiment, the pre-trigger TTL signal of the femtosecond laser was used to trigger the high-voltage power supply to realize the synchronization of the discharge and the laser signal. Under the same electrodes distance, femtosecond laser was used to guide high-voltage discharge (Fig. 2d). As can be seen in Fig. 2(d), a straight and bright discharge arc was formed between the two electrodes, the discharge path was not random and completely along the plasma channel generated by femtosecond laser, and the brightness was darker than that of free discharge. The main reason for this phenomenon is that the resistance of the plasma channel generated by the femtosecond laser through the self-focusing effect is relatively small, so that the charging voltage at both ends of the electrode is less than the one during free discharge. Therefore, the precise control of high-voltage discharge in space and time can be realized using the plasma channel generated by femtosecond laser.

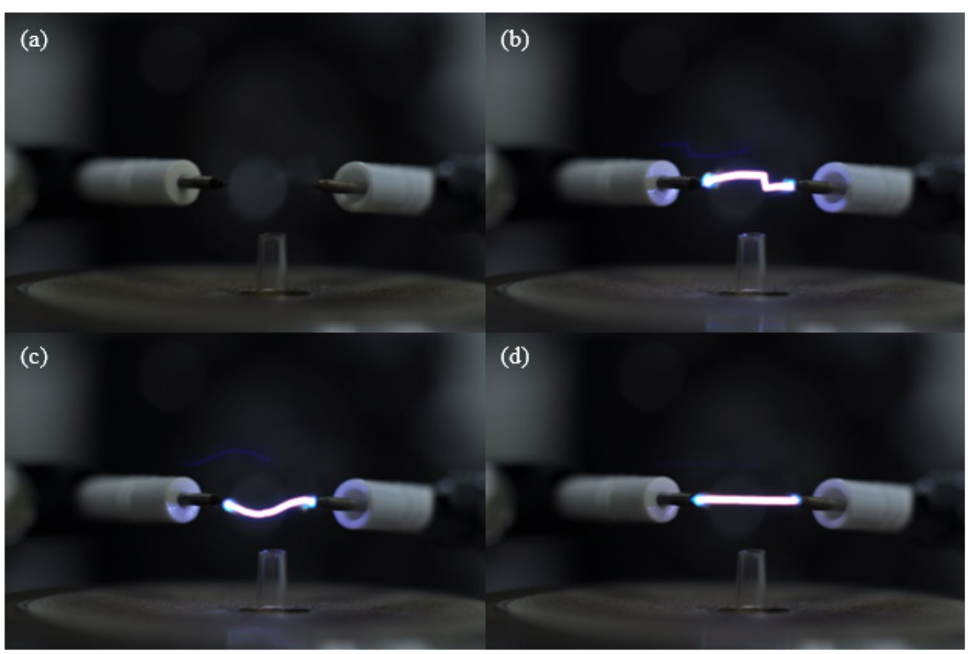

Fig. 2 Photos of free discharge and femtosecond laser-guided high-voltage discharge. **a** Electrodes and nozzle; **b**, **c** free discharge; **d** guide discharge

Meanwhile, it can be observed in Fig. 2(d) that the discharge arc between the two electrodes was within a certain spatial range, and the plasma intensity remained basically unchanged. This indicated that the filament plasma induced by the femtosecond laser-guided high-voltage discharge had a one-dimensional uniformity, and hence one-dimensional and simultaneous multi-component measurement can be achieved by obtaining the space-resolved spectrum of the filamentous plasma.

3 Results and discussion

3.1 SF_6 discharge decomposition spectral analysis

The plasma spectrum of pure SF_6 (concentration of 99.999%) was detected by the above experimental device with the discharge voltage of 14 kV, as shown in Fig. 3. The photo of filament was obtained with a single-lens reflex camera as shown in Fig. 3(a). The white arrow in the figure indicates the laser direction, and the blue area in the white dotted line is the plasma channel generated by the femtosecond laser focusing. The signal in this area was collected by the spectrometer slit and imaged by the ICCD camera (Fig. 3b). The camera gate width is 100 μs, the gain is 50, and the read and write delay is 0 ns (relative to the laser signal, the laser signal appears at 3130 ns, triggering high-voltage power supply at about 3230 ns, the same below). In Fig. 3(b), the abscissa represents the wavelength and the ordinate represents the radial distance. From top to bottom is the direction of femtosecond laser incidence. It can be clearly seen in Fig. 3(b) that the plasma channel imaging area was divided into the SF_6 area and the surrounding air area. The emission spectrum of SF_6 region was integrated radial to obtain the emission spectra of SF_6 decomposition products, as shown in Fig. 3(c). In Fig. 3(c), it is observed that there are a large number of S and F atoms and ions lines in the SF_6 region, including emission lines of fluorine (spectral range 638–691 nm) and sulfur (spectral range 520–550 nm), which are difficult to be observed as described in literature [22]. The emission line of Fe is generated by electrode materials, and different atoms and ions lines are marked with different colors in the figure. The inset shows the attribution of various valence ions spectral lines of S in the wavelength of 340–420 nm. Analysis of the spectra indicated that a large number of S and F atoms and ions were generated by decomposition of SF_6 gas under discharge, and that femtosecond laser-guided high-voltage discharge technology can be used to realize real-time on-line detection of SF_6 decomposition products, namely in situ measurement.

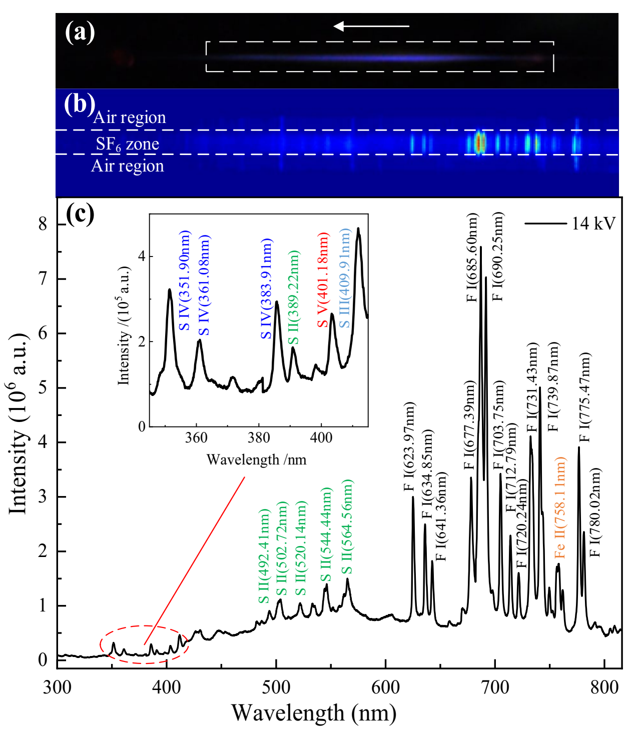

Fig. 3 SF_6 decomposition spectrum of femtosecond laser-guided high-voltage discharge. **a** Filament; **b** spatially resolved spectrum; **c** SF_6 plasma spectrum

The main generation processes of S and F atoms and ions are as follows: first, SF_6 gas molecules are collided by high-energy electrons generated by a high-energy electric field and then decompose, producing some F atoms and low-fluorine sulfides, as shown in chemical reaction (1). At the same time, the generated low-fluorine sulfide will be further decomposed by the impact of high-energy electrons to produce S and F atoms, as illustrated in the chemical reaction formula (2). Finally, the collision of the generated S atoms by high-energy electrons will further generate S ions, that is, the S band of 300–550 nm in Fig. 3(c), and the corresponding reaction processes are chemical reaction (3):

$$SF_6 + e \rightarrow SF_x + (6 - x)F \quad (x = 0, 1 \ldots 5), \tag{1}$$

$$SF_x + e \rightarrow S + xF \quad (x = 0, 1 \ldots 5), \tag{2}$$

$$S + e \rightarrow S^{x+} \quad (x = 1,\ 2 \ldots 4). \tag{3}$$

3.2 Spectral analysis of SF_6 discharge decomposition at different voltages

To study the effects of voltage intensity on SF_6 decomposition products, different voltages were applied to the electrodes. Figure 4 shows the decomposition spectrum of SF_6 at different voltages. It can be seen in Fig. 4 that the profile of the SF_6 decomposition spectrum at different voltages was the same as that in Fig. 3. The inset shows the spectrum

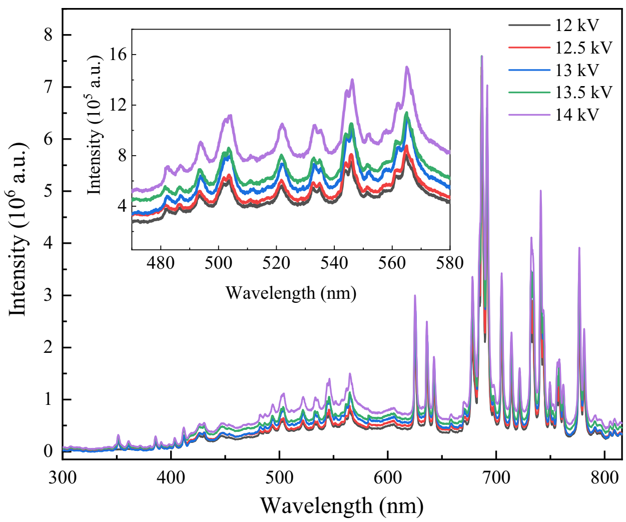

Fig. 4 SF_6 decomposition spectrum at different voltages

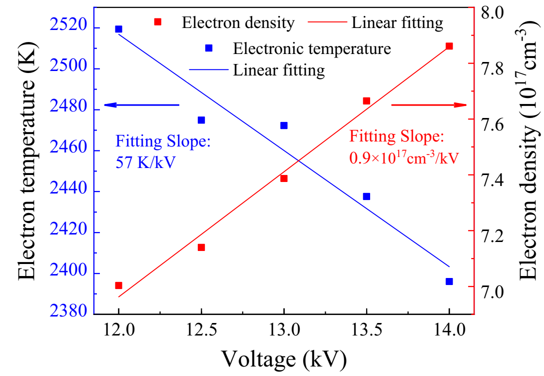

Fig. 5 Electron density and electron temperature of SF_6 plasma under different discharge voltages

in the wavelength ranges from 340 to 380 nm. From the inset, it can be clearly seen that the intensity of spectrum lines increased with the increase of the discharge voltage, the potential difference formula (formula (4)), the electron kinetic energy formula (Eq. (5)) and random thermal motion of electrons can explain this phenomenon:

$$U = E\lambda, \tag{4}$$

$$mv^2/2 = eU, \tag{5}$$

where U is the potential difference, E is the electric field intensity, and λ is the electron mean free path. m, v, and e are the electron mass, the electron velocity and the electron charge, respectively.

It can be seen from Eqs. (4) and (5) that the increasing discharge voltage caused an increase in the electric field intensity (E) between the electrodes, and hence the energy obtained by electrons was higher. In addition, as the discharge voltage increased, the random thermal motion of electrons became severe and the ion diffusion effect was enhanced. Eventually, the impact excitation cross section of S and F atoms and ions generated by electron collision with SF_6 was increased, and more excited S and F atoms and ions were generated, resulting in an increased intensity of each atom and ion line in the spectrum.

In addition, it can be seen in Figs. 3 and 4 that there is a great difference between the intensities of each line of S or F at different wavelengths, which is mainly because the upper level excitation energy and transition probabilities of S or F atoms or ions at different wavelengths are not identical. For example, the F atom at 685.60 nm had a higher transition probability than F atoms at other wavelengths, and its upper level excitation energy was the lowest, that is, the required electron excitation energy was the lowest, so its spectral line intensity was the highest. In contrast, the F atom at 720.24 nm had a lower transition probability than the F atom at other wavelengths, and its upper level excitation energy was the highest, so its line intensity was low.

3.3 Analysis of SF_6 discharge decomposition parameters

Electron temperature and electron density are two important and basic parameters of discharge plasma, which are of great significance for understanding the discharge process and plasma characteristics.

3.3.1 Analysis of SF_6 plasma electron density

Assuming that SF_6 arc plasma meets local thermodynamic equilibrium (LTE) [23], the plasma electron density can be solved by formula (6) [24–26]:

$$\Delta\lambda_{1/2} = 2\omega N_e/10^{16}, \tag{6}$$

where $\Delta\lambda_{1/2}$ and ω are emission spectra line FWHM (the full width half maximum) and the electron collision parameter respectively. N_e is the requested electron density.

The electron density was calculated using the F I 685.60 nm spectral line with the highest signal-to-background ratio, and fit the F atomic line at 685.60 nm by Lorentz fitting to obtain the FWHM of the line. From Eq. (6), the electron density of SF_6 plasma at different discharge voltages can be obtained, as shown in Fig. 5. As can be seen in Fig. 5, the electron density of SF_6 plasma increased linearly with the increase of the discharge voltage between the two electrodes. It can be explained the increasing discharge voltage caused the physicochemical reaction between the two electrodes to become more intense, the ionization of SF_6 gas increased, and hence the number of electrons increased accordingly. Fitting it with a straight line, the slope of the straight line is 0.9×10^{17} cm^{-3}/kV, indicating that for every 1 kV increase in discharge voltage, the plasma electron density increases by 0.9×10^{17} cm^{-3}.

3.3.2 Analysis of SF_6 plasma electron temperature

At the condition that SF_6 plasma satisfies the LTE, the plasma electron temperature can be solved by Boltzmann multispectral slope method [26–28]:

$$\ln\left(\frac{I\lambda}{A_{ik}g_k}\right) = -\frac{E_k}{kT_e} + C, \tag{7}$$

where I, λ, A_{ik}, g_k, E_k, and k are the corresponding spectral line relative intensity, center wavelength, transition probability, statistical weight of the upper level, upper level excitation energy, and the Boltzmann constant. T_e is the requested electron temperature.

Taking E_k as the abscissa and $\ln\left[I\lambda/(A_{ik}g_k)\right]$ as the ordinate to obtain a series of scatter plots, linearly fitting the discrete points to obtain the slope of the straight line, and the electronic temperature can be further obtained by the straight line slope ($-1/kT_e$). In the calculation of the plasma electron temperature, the greater the difference in upper level excitation energy on the spectral line, the more accurate the calculation result. According to the experimental data, therefore, three emission lines of F atoms (623.97 nm, 677.40 nm and 703.75 nm) were chosen to calculate T_e, and the electron temperature of SF_6 plasma at different discharge voltages is shown in Fig. 5.

It can be seen in Fig. 5 that as the discharge voltage increased, the electron temperature decreased linearly. This is mainly because an increase in discharge voltage led to an increased density of gas molecules generated by SF_6 decomposition, and the average free path of electrons decreased. At the same time, the random thermal motion of the electrons became more intense with increasing discharge voltage, the number of electron collisions per unit distance increased as the result of the intensified collision between the particles, and hence the energy loss during the movement of the electrons increased, which eventually caused the temperature of the electrons to decrease. Fitting it with a straight line, the linear slope is 57 K/kV, indicating that the plasma electron temperature decreases by 57 K/kV for every 1 kV increase in discharge voltage.

3.3.3 Analysis of the LTE

Mc Whirter criterion is used to determine whether the plasma is in the LTE [26, 29]:

$$N_e > 1.6 \times 10^{14} T_e^{1/2} (E_k - E_i)^3 \text{ cm}^{-3}, \tag{8}$$

where N_e, T_e, E_k, and E_i are the corresponding spectral line electron density, electron temperature, upper level excitation energy and lower energy level. In this experiment, the maximum difference in excitation energy between the upper and lower energy levels of the spectral line is 1.93 eV, the maximum electron temperature is 2519 K, and the minimum electron density satisfying the LTE is 0.58×10^{17} cm^{-3}, and the minimum electron density obtained in the experiment is 7×10^{17} cm^{-3}, which obviously meets Mc Whirter criterion that SF_6 plasma is in the LTE.

4 Conclusions

In this paper, femtosecond laser-guided high-voltage discharge technology has been used to study the emission spectrum characteristics of SF_6 plasma. The spectral analysis of the SF_6 decomposition products indicated that the decomposition products contained a lot of S and F atoms and ions. The S and F atoms were mainly generated directly or indirectly by high-energy electrons colliding with SF_6, and S ions were generated by S atoms being collided by high-energy electrons. The intensity of different lines was different, and the analysis illustrated that it was affected by different transition probabilities and the effect of excitation energy at the upper level. Based on the SF_6 decomposition spectrum under different discharge voltages, it is found that the maximum difference in excitation energy between the upper and lower energy levels of the spectral line is 1.93 eV, the maximum electron temperature is 2519 K. Moreover, the minimum electron density satisfying the LTE is 0.58×10^{17} cm^{-3}, and the minimum electron density obtained in the experiment is 7×10^{17} cm^{-3}. Furthermore, the intensity of each atom and ion line of the SF_6 discharge decomposition spectrum increased as the discharge voltage increased. Besides, the electron temperature and electron density of SF_6 plasma at different voltages have been studied. The increasing discharge voltage caused the electron density to increase linearly, and the electron temperature to decrease linearly. The analysis showed that an increase in the discharge voltage resulted in a violent physicochemical reaction between the two electrodes, which caused the ionization of SF_6 gas to increase, and hence electron density increased accordingly. As the voltage rose, the random thermal motion of the electrons increased, which caused the collision between particles to intensify. Consequently, the energy loss during the movement of the electrons increased, eventually causing the electron temperature to decrease. It is proved that the SF_6 plasma was in the LTE based on the Mc Whirter criterion. The results are of great significance for studying the decomposition mechanism of SF_6 and the on-line monitoring technique of high-voltage equipment.

Acknowledgements This work was supported by the National Natural Science Foundation of China (Grant Nos. 62175208 and 518061495) and the Central Government Guides Local Science and Technology Development Foundation (Grant No. 216Z1701G) and the Natural Science Foundation of Hebei Province (Grant No. F2021203052).

Declarations

Conflict of interest The authors declare no conflict of interest.

References

1. G.M. Wang, H.E. Jo, S.J. Kim, S.W. Kim, G.S. Kil, Measurement and analysis of partial discharges in SF_6 gas under HVDC. Measurement **91**, 351–359 (2016)
2. X.X. Zhang, Y. Zhang, S.Y. Zhou, Z. Wei, Y. Wang, Y.F. Wang, The detection and quantification of heptafluoroisobutyronitrile (C_4F_7N) and its decomposition products by infrared spectroscopy and chemometrics. Spectroc. Acta Pt. A-Molec. Biomolec. Spectr. **233**, 118161 (2020)
3. Q.Q. Gao, X.H. Wang, A.J. Yang, C.P. Niu, M.Z. Rong, L.L. Jiao, Q. Ma, Influence of H_2O and O_2 on the main discharge mechanism in 50 Hz ac point-plane corona discharge. Phys. Plasmas. **26**(3), 033508 (2019)
4. Q.Q. Gao, C.P. Niu, X.H. Wang, A.J. Yang, Y. Wu, A.B. Murphy, M.Z. Rong, X.X. Fu, J.L. Liu, Y.B. Xu, Chemical kinetic modeling and experimental study of SF_6 decomposition byproducts in 50 Hz ac point-plane corona discharge. J. Phys. D **51**(29), 295202 (2018)
5. Z.J. Wei, Q. Zhou, W. Zeng, Hierarchical WO_3-NiO microflower for high sensitivity detection of SF_6 decomposition byproduct H_2S. Nanotechnology **31**(21), 215701 (2020)
6. X.X. Zhang, Z.L. Cui, Z. Cheng, Y.L. Lia, H. Xiao, Quantitative detection of H_2S and CS_2 mixed gases based on UV absorption spectrometry. RSC Adv. **7**(80), 50889–50898 (2017)
7. Z.L. Cui, X.X. Zhang, Z. Cheng, Y.L. Li, H. Xiao, Quantitative analysis of SO_2, H_2S and CS_2 mixed gases based on ultraviolet differential absorption spectrometry. Spectroc. Acta Pt. A-Molec. Biomolec. Spectr. **215**, 187–195 (2019)
8. F.P. Zang, J. Tang, H.J. Sun, J.Y. Pan, Q. Yao, J.J. He, X.Z. Hou, Quantitative analysis of the influence of regularity of SF_6 decomposition characteristics with trace O_2 under partial discharge. IEEE Trns. Dielectr. Electr. Insul. **21**(4), 1462–1470 (2014)
9. J. Tang, F.P. Zeng, X.X. Zhang, J.Y. Pan, Q. Yao, X.Z. Hou, Y. Tang, Relationship between decomposition gas ratios and partial discharge energy in GIS, and the influence of residual water and oxygen. IEEE Trns. Dielectr. Electr. Insul. **21**(3), 1226–1234 (2014)
10. R.J. van Brunt, J.T. Herron, Plasma chemical model for decomposition of SF_6 in a negative glow corona discharge. Phys. Scr. T **53**, 9–29 (1994)
11. J. Tang, F. Liu, X.X. Zhang, Q.H. Meng, J.B. Zhou, Partial discharge recognition through an analysis of SF_6 decomposition products part 1: decomposition characteristics of SF_6 under four different partial discharges. IEEE Trns. Dielectr. Electr. Insul. **19**(1), 29–36 (2012)
12. J. Tang, F. Liu, X.X. Zhang, Q.H. Meng, J.B. Zhou, Partial discharge recognition through an analysis of SF_6 decomposition products part 2: feature extraction and decision tree-based pattern recognition. IEEE Trns. Dielectr. Electr. Insul. **19**(1), 37–44 (2012)
13. F.Y. Chu, SF_6 decomposition in gas-Insulated equipment. IEEE Trns. Dielectr. Electr. Insul. **2EI-21**(5), 693–725 (1986)
14. Z. Li, S.Y. Chen, S.K. Gong, B. Feng, Z. Zhou, Theoretical study on gas decomposition mechanism of SF_6 by quantum chemical calculation. Comput. Theor. Chem. **1088**, 24–31 (2016)
15. B. Li, D.Y. Zhang, J.X. Liu, Y.F. Tia, Q. Gao, Z.S. Li, A review of femtosecond laser-induced emission techniques for combustion and flow field diagnostics. Appl. Sci.-Basel. **9**(9), 1906 (2019)
16. P. Polynkin, Multi-pulse scheme for laser-guided electrical breakdown of air. Appl. Phys. Lett. **111**(16), 161102 (2017)
17. S.B. Leonov, A.A. Firsov, M.A. Shurupov, J.B. Michael, M.N. Shneider, R.B. Miles, N.A. Popov, Femtosecond laser guiding of a high-voltage discharge and the restoration of dielectric strength in air and nitrogen. Phys. Plasmas. **19**(12), 123502 (2012)
18. G. Méjean, R. Ackermann, J. Kasparian, E. Salmon, J. Yu, J.P. Wolf, K. Rethmeier, W. Kalkner, P. Rohwetter, K. Stelmaszczyk, L. Wöste, Improved laser triggering and guiding of megavolt discharges with dual fs-ns pulses. Appl. Phys. Lett. **88**(2), 021101 (2016)
19. M. Rodriguez, R. Sauerbrey, H. Wille, L. Wöste, T. Fuji, Y.B. André, A. Mysyrowicz, L. Klingbeil, K. Rethmeier, W. Kalkner, J. Kasparian, E. Salmon, J. Yu, J.P. Wolf, Triggering and guiding megavolt discharges by use of laser-induced ionized filaments. Opt. Lett. **27**(9), 772–774 (2002)
20. L. Arantchouk, A. Houard, Y. Brelet, J. Carbonnel, J. Larour, Y.B. André, A. Mysyrowicz, A simple high-voltage high current spark gap with subnanosecond jitter triggered by femtosecond laser filamentation. Appl. Phys. Lett. **102**(16), 163502 (2013)
21. B. Li, Y.F. Tian, Q. Gao, D.Y. Zhang, X.F. Li, Z.F. Zhu, Z.S. Li, Filamentary anemometry using femtosecond laser-extended electric discharge—FALED. Opt. Express. **26**(16), 21132–21140 (2018)
22. S. Eschlböck-Fuchs, P.J. Kolmhofer, M.A. Bodea, J.G. Hechenberger, N. Huber, R. Roessler, J.D. Pedarnig, Boosting persistence time of laser-induced plasma by electric arc discharge for optical emission spectroscopy. Spectroc. Acta Pt. B-Atom. Spectr. **109**, 31–38 (2015)
23. S. Vacquie, A. Gleizes, H. Kafrouni, Measurements of electron density in a SF_6 arc plasma. J. Phys. D: Appl. Phys. **18**(11), 2193–2205 (1985)
24. Y.F. Liu, Y.J. Ding, Z.M. Peng, Y. Huang, Y.J. Du, Spectroscopic study on the time evolution behaviors of the laser-induced breakdown air plasma. Acta Phys. Sin. **63**(20), 205205 (2014)
25. J. Xu, Y. Luo, L. Zhu, J.T. Han, D. Chen, Effect of shielding gas on the plasma plume in pulsed laser welding. Measurement **134**, 25–32 (2019)
26. L. Wang, Y.X. Fu, L. Xu, H. Gong, C.C. Rong, The effect of sample temperature on characteristic parameters of the nanosecond laser-Induced Cu plasma. Spectrosc. Spectr. Anal. **39**(4), 1247–1251 (2019)
27. Y.M. Huang, S.S. Li, J.H. Li, H.B. Chen, L.J. Yang, S.B. Chen, Spectral diagnosis and defects prediction based on ELM during the GTAW of Al alloys. Measurement **136**, 405–414 (2019)
28. P. Christopher, S. Mikhail, M. Richard, Kinetics model of femtosecond laser ionization in nitrogen and comparison to experiment. J. Appl. Phys. **125**(24), 5098306 (2019)
29. C. Pagano, S. Hafeez, J.G. Lunney, Influence of transverse magnetic field on expansion and spectral emission of laser produced plasma. J. Phys. D: Appl. Phys. **42**(15), 155205 (2009)